Applied Catalysis B: Environmental 130–131 (2013) 1–7

Contents lists available at SciVerse ScienceDirect

Applied Catalysis B: Environmental

journal homepage: www.elsevier.com/locate/apcatb

BiOI thin film via chemical vapor transport: Photocatalytic activity, durability, selectivity and mechanism

Liqun Ye[a], Junnian Chen[a], Lihong Tian[a], Jinyan Liu[a], Tianyou Peng[a], Kejian Deng[b], Ling Zan[a,*]

[a] College of Chemistry and Molecular Science, Wuhan University, Wuhan 430072, People's Republic of China
[b] Key Laboratory of Catalysis and Materials Science of the State South-Central University for Nationalities, Wuhan 430074, People's Republic of China

ARTICLE INFO

Article history:
Received 15 August 2012
Received in revised form 9 October 2012
Accepted 14 October 2012
Available online 23 October 2012

Keywords:
BiOI
Photocatalytic
Durability
Selectivity
Mechanism

ABSTRACT

BiOI thin film (BiOI TF) was prepared via a low temperature chemical vapor transport (CVT) route for the first time, and characterized by X-ray diffraction, X-ray photoelectron spectroscopy, field emission scanning electron microscopy, transmission electron microscopy, high-resolution transmission electron microscopy, fast-Fourier transform pattern and UV–vis diffuse reflectance. As-synthesized BiOI thin film was composed of high symmetrical BiOI nanosheets with dominant exposed {0 0 1} facets. It displayed better photocatalytic activity, durability and selectivity than benchmark P25 TiO_2 thin film and the origin come from the layered structure and good photoelectrochemical performance, CVT immobilization, the 100% terminal oxygen atoms of {0 0 1} facets, respectively. At end, the photocatalytic mechanism with $O_2^{\bullet-}$ production was studied.

1. Introduction

BiOI is an important V-VI-VII ternary semiconductor compound with suitable absorption edge at about 670 nm and the estimated band gap energy of about 1.8 eV.[1–9] It is known as a tetragonal layered structure with lattice constants of $a = 0.3994$ nm and $c = 0.9149$ nm (Fig. S1a). The enough large space of BiOI layered structure can polarize the related atoms and orbital and induce the presence of internal static electric fields perpendicular to the $[Bi_2O_2]$ slabs and halogen anionic slabs in BiOI. At end, effective separation of the photoinduced electron–hole pairs along the [0 0 1] direction can be displayed (Fig. S1b). On the other hand, BiOI has an indirect-transition band-gap so that the excited electron has to travel certain k-space distance to be emitted to valence band (VB) which reduces the recombination probability of the excited electron and the hole.[3,4] So, BiOI can be used as an excellent semiconductor material for solar utilization. Furthermore, our previous study about BiOI nanosheets showed that the {0 0 1} facet-dependent photoactivity of BiOI was found and explained the origin: photoinduced oxygen vacancies and self-induced internal electric fields result in high separation efficiency of photogenerated electron and hole.[3,4,10,11]

BiOI photocatalyst is usually used in the powdered form, which has to be separated from the water in a slurry system after photocatalytic reaction and is inconvenient for many practical applications.[3–9] Immobilizing BiOI powder as thin films on a solid substrate can overcome it. However, to the best of our knowledge, there are still no reports about on the BiOI thin films (BiOI TF) for photocatalytic reaction. Most of the reported methods for the synthesis of BiOI nanostructures are wet chemical methods, such as solvothermal method[12–14] and reverse microemulsions.[15] However, they are difficult to form thin films by these methods. Vapor-phase synthesis has been shown to be a powerful method for the synthesis of high quality nanostructures thin films,[16–20] but this method has not yet been applied to BiOI nanostructures.

Selectivity also is a very important factor for catalytic process. Photocatalytic selectivity of alcohols and azo dyes in TiO_2 system have been paid more attention.[21–25] However, pure TiO_2 shows poor photocatalytic selectivity, due to the adsorption selectivity is very low. For obationing high photocatalytic selectivity, TiO_2 is usually modified by fluorin or alkali to enhance the adsorption selectivity. The surface atoms structural reveal that the {0 0 1} facets of BiOI contains 100% terminal oxygen atoms, and {0 0 1} facets are expected to be more negatively charged. So, BiOI nanosheets with dominant exposed {0 0 1} facets may can show adsorption selectivity for azo dyes and result in high photocatalytic selectivity.

In this paper, we exploit a chemical vapor transport (CVT) synthesis of high quality BiOI nanostructures thin film with {0 0 1} facets exposing by chemical vapor transport of BiI_3 powders at relatively low temperature (250 °C). As-synthesized BiOI TF shows much higher photocatalytic activity, durability and selectivity than

* Corresponding author.
E-mail address: irlab@whu.edu.cn (L. Zan).

0926-3373/$ – see front matter © 2012 Elsevier B.V. All rights reserved.
http://dx.doi.org/10.1016/j.apcatb.2012.10.011

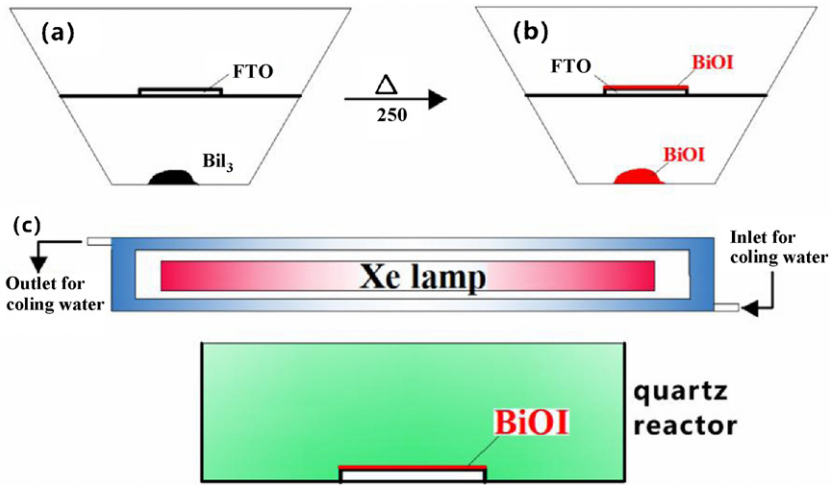

Scheme 1. Schematic illustrations of BiOI thin films via a CVT process: (a) before CVT and (b) after CVT, and (c) schematic illustration photocatalytic experiments.

P25 TiO_2 thin film (TiO_2 TF). At end, the photocatalytic mechanism with $O_2^{\bullet-}$ production was researched.

2. Experimental

2.1. Preparation

Firstly, the FTO conducting glass (fluorine-doped tin oxide glass, 15–20 Ω sq.$^{-1}$) was cleaned by isopropanol and ethanol. BiOI thin films (BiOI TFs) were prepared via a CVD route as shown in Scheme 1. 0.5 g BiI_3 (analytical pure, Aladdin Chemistry Co., Ltd.) was added into a ceramic crucible and a conducting glass was layed on the center of the ceramic crucible (Scheme 1a). Then, put the ceramic crucible into a muffle furnace and increase temperature to 250 °C with the heating rate of 2 °C min^{-1}. At end, the CVD process was performed under air atmosphere for 3 h, which was followed by cooling at room temperature.

For comparison, P25 TiO_2 thin film (TiO_2 TF) was prepared as following: a 1.0 g TiO_2 was mixed with 4.0 mL of ethanol, by ball-milling for 10 h. The obtained paste was spread on a clean FTO glass using the doctor blading technique. After drying in atmosphere, the film was sintered at 300 °C for 2 h.

2.2. Characterization

X-ray diffraction (XRD) pattern were recorded on a Bruker D8 advance X-ray diffractometer by using Cu Kα radiation and 2θ scan rate of 6°/min. UV–vis diffuse reflectance spectra (DRS) were obtained using a Shimadzu UV-3600 spectrometer by using $BaSO_4$ as a reference. FESEM images were obtained by a JEOL JEM-6700F field emission scanning electron microscope with operating at an accelerating voltage 5 kV and applied current 10 mA. HRTEM image was obtained by a JEOL JEM-2010FEF field emission electron microscope with operating at an accelerating voltage of 200 kV. X-ray photoelectron spectroscopy (XPS) measurements were carried out by a VG Multilab 2000 spectrometer (Thermo Electron Corporation) with an Ar Kα X-ray source, and the spectra calibrated to the C 1s peak at 284.6 eV.

2.3. Photoelectrochemical measurements

The identical platinized FTO counter-electrode was placed over the BiOI TF electrode, and the electrolyte (containing 0.5 M LiI, 0.05 M I_2, and 0.1 M 4-tert-butylpyridine in 1:1 acetonitrile–propylene carbonate) was sandwiched between the photoanode and the platinized counter-electrode by firm press. An adhesive tape (approximately 50 μm) was placed between the photoanode and the counter-electrode to avoid short-circuiting.

The BiOI electrode was illuminated by light with energy of 100 mW cm^{-2} (1.5 G simulated sunlight) from a 500 W Xe-lamp. The light intensity was determined using a SRC-1000-TC-QZ-N reference monocrystalline silicon cell system (Oriel, U.S.), which was calibrated by National Renewable Energy Laboratory, A2LA accreditation certificate 2236.01. Computer-controlled Keithley 2400 source meter was employed to collect the current–voltage (I–V) curves of BiOI electrode. The active area was 5 mm × 5 mm.

2.4. Photocatalytic activity test

The photoactivity was evaluated by the degradation of RhB under UV–vis light irradiation. The light was obtained by a 500 W high-pressure Xenon lamp. The lamps were bought from Changzhou Yuyu Electro-Optical Device Co., Ltd. China. Typical photocatalytic degradation process is arranged in such a way: 50 mL aqueous suspensions (5 mg/L RhB or mixed solution of 5 mg/L MB and 10 mg/L MO) placed in a quartz reactor, and then BiOI TF or TiO_2 TF were added as shown in Scheme 1c. The natural pH of the dispersed photocatalyst/RhB solution was around pH 6. Two additional experiments under acid conditions were carried out at pH 4 by adding 4 M HNO_3. In the same way, experiments under basic conditions were performed at pH 8 and 10. In these cases, a 4 M NaOH solution was used to reach these basic conditions. Prior to irradiation, the quartz beaker was put in dark for 30 min to get desorption–adsorption equilibrium. At certain time intervals, 4 mL solution were sampled and analyzed by recording the maximum absorption band (554 nm for RhB, 665 nm for MB and 465 nm for MO) and UV–visible spectra of dyes using a Shimadzu UV-3600 spectrophotometer. Total dissolved organic carbon was determined using TOC Analyzer (Shimadzu TOV-VCPH).

2.5. Photocatalytic mechanism

For detecting the active species during photocatalytic reactivity, hydroxyl radicals (•OH), superoxide radical ($O_2^{\bullet-}$) and holes (h^+) were investigated by adding 1.0 mM IPA (a quencher of •OH), BQ (a quencher of $O_2^{\bullet-}$) and TEOA (a quencher of h^+), respectively.[26,27] The method was similar to the former photocatalytic activity test.

NBT (2.5×10^{-5} mol/L, exhibiting an absorption maximum at 259 nm) was used to determine the amount of $O_2^{\bullet-}$ generating from BiOI TF photocatalytic system. The production of $O_2^{\bullet-}$ was

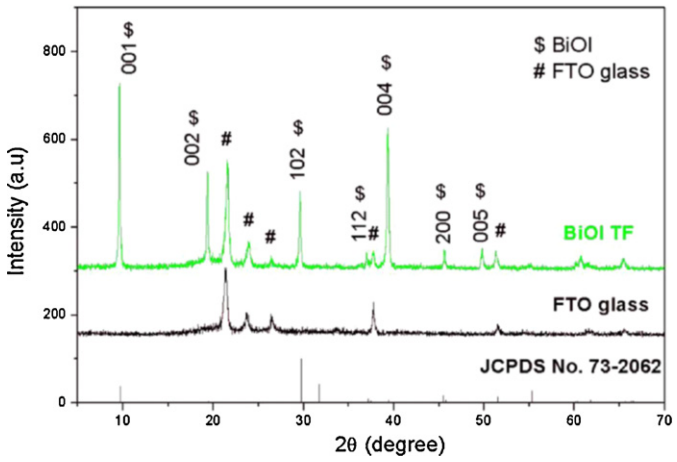

Fig. 1. XRD pattern of the bare FTO glass and BiOI TF.

quantitatively analyzed by detecting the concentration of NBT with Shimadzu UV-3600 spectrophotometer. The method was similar to the former photocatalytic activity test with NBT replacing the RhB. The $O_2^{\bullet-}$ production under different monochromatic light wavelength of 400 and 550 nm were measured.[26,27]

3. Results and discussion

3.1. Catalyst characterization

Fig. 1 shows X-ray diffraction (XRD) pattern of BiOI TF sample. These peaks at 9.6° (0 0 1), 19.3° (0 0 2), 29.6° (0 1 2), 31.8° (1 1 0), 37.1° (0 1 3), 39.4° (0 0 4), 45.6° (0 2 0) and 49.8° (1 2 2) are indexed to that of tetragonal BiOI (JCPDS file No. 73–2062). No residual BiI_3, Bi_2O_3 and Bi_5O_7I phase was detected. This indicates that as-synthesized BiOI is pure BiOI. The XPS measurements provided further information for the evaluation of the purity and surface composition of the BiOI nanosheets. The XPS survey spectrum in Fig. S2a demonstrates no peaks of other elements than C, O, Bi and I in the sample, a proof of the purity of BiOI nanosheets. Fig. 2b shows the high- resolution XPS spectra of Bi4f. The two strong peaks at the Bi region of 159.1 and 164.4 eV are respectively assigned to Bi4f7/2 and Bi4f5/2 of BiOI.

Fig. 2a–c shows the field emission scanning electron microscope (FESEM) images BiOI TF. After CVT, it can be found most are symmetrical BiOI single-crystal nanosheets (Fig. 2a). The side view of BiOI TF (Fig. 2b) also supports BiOI nanosheets being deposited on FTO in comparison to the bare FTO glass (Fig. S3). And the thickness of BiOI thin film is about 690 nm. Usually, BiOI is in the morphologies of nanoflakes, nanoplates, aggregative spheres or nanometer particles. Here, BiOI displayed single-crystal nanosheets with high symmety in Fig. 2c. It can be found that the thickness BiOI nanosheets are from 10 nm to 30 nm. An angle of 90°, which is consistent with the theoretical interfacial angle between {1 1 0} and {1 −1 0} facets, was observed. It indicates that the top and bottom surfaces are {0 0 1} facets as we desire. On the basis of FESEM analysis, it can be suggested that BiOI TF has high percentage of {0 0 1} facets.

To further obtain the morphology and structure information, the transmission electron microscope (TEM) and high-resolution transmission electron microscope (HRTEM) analysis of BiOI nanosheets have been applied. TEM image also shows an angle of 90° between {1 1 0} and {1 −1 0} facets (Fig. 2d). The HRTEM image of a single BiOI crystal (Fig. 2e, viewed from the [0 0 1] axis) shows clearly two sets of lattice fringes with a lattice spacing of 0.28 nm, corresponding to that of the {1 1 0} and {1 −1 0} facets and as shown

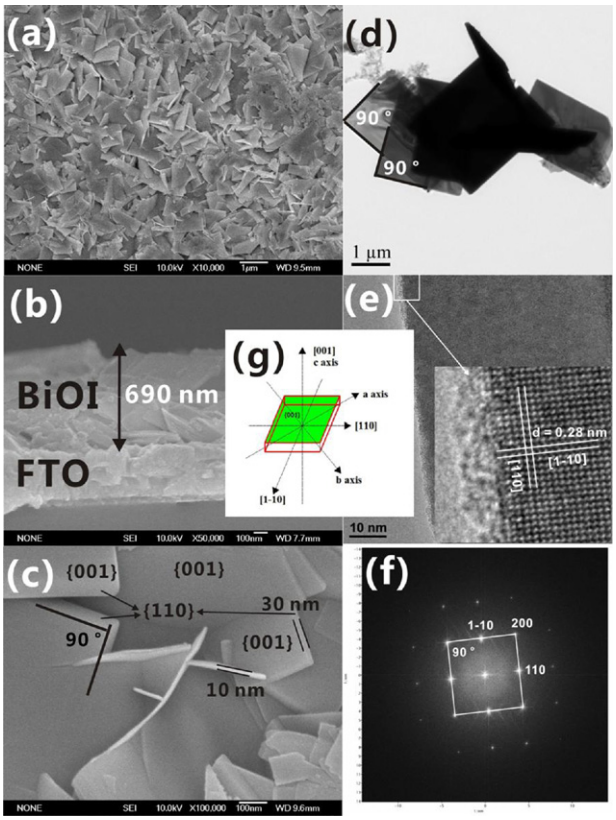

Fig. 2. (a) Top view FESEM image of BiOI TF; (b) side view FESEM image of BiOI TF; (c) FESEM image of BiOI nanosheets; (d) TEM image of BiOI nanosheets; (e) HRTEM images of BiOI nanosheets; (f) FFT image of BiOI nanosheets; and (g) the simulation model of BiOI nanosheets.

in Fig. 2f, the angle labeled in the corresponding fast-Fourier transform pattern (FFT) image is 90°. They are identical to the theoretical value for the angle between the {1 1 0} and {1 −1 0} facets. These results also prove that the BiOI single crystal exhibits the two flat {0 0 1} facets. Fig. 2g gives a simulation illustration of the BiOI single-crystal nanosheets.

The heating rate and temperature of CVT affect the morphology of BiOI TF. Fig. S4a shows the FESEM image of BiOI TF with heating rate of 1 °C min^{-1} to 250 °C. Compare with heating rate of 2 °C min^{-1} to 250 °C, it can be found that the nanosheets are larger and thicker, which indicates that low heating rate can enhance the crystallinity. However, it can be found that the BiOI nanosheets cannot cover the surface of FTO glass. Fig. S4b displays the FESEM images of BiOI TF with temperature of 300 °C with 2 °C min^{-1}. It can be seen that most are broken nanoplates, which result in low symmetrical BiOI single-crystal nanosheets. It implies that higher CVT temperature is a disadvantage for symmetry and {0 0 1} facets exposure.

Fig. 3a shows the UV–vis absorption spectra of BiOI nanosheets. There is an absorption edge around 620 nm and by extrapolating the linear region of a plot of the absorbance squared versus energy, the band gap is estimated to be 1.79 eV. This observed bandgap agrees well with the previous reports.[4,12] Red BiOI film can absorb most of visible light and be excited under sunlight irradiation. Fig. 3b shows the current–voltage characteristics of the BiOI TF electrode. The dark current of BiOI TF electrode was neglected. Interestingly, the BiOI TF electrode exhibits remarkable photocurrents compared with the dark currents and TiO_2 TF electrode (the inset image of Fig. 3b). This indicates that the BiOI TF could effectively absorb the photons and transfer them into electricity as the photovoltaic effect. The efficiencies (η) are

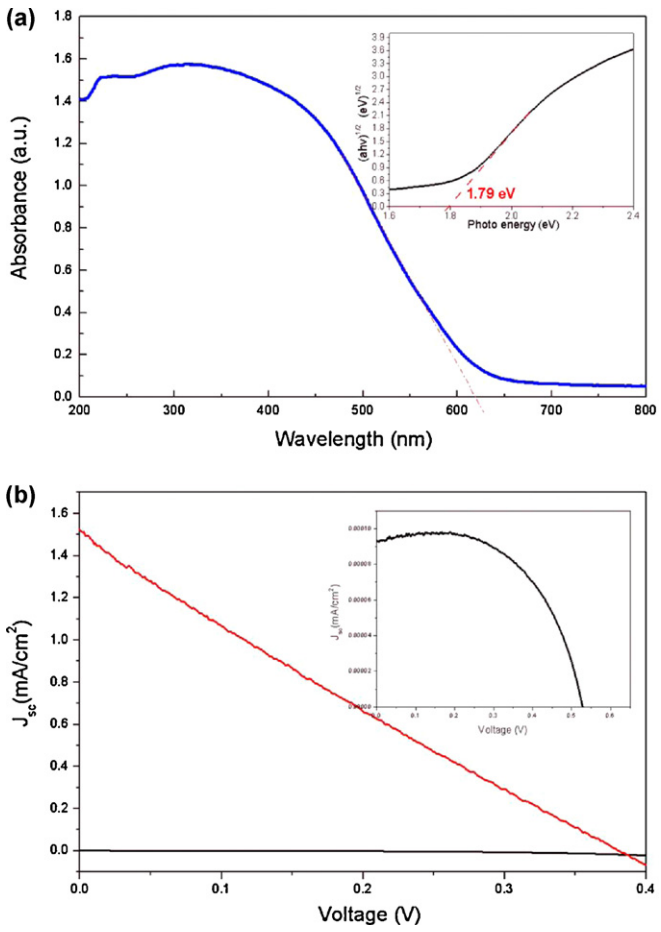

Fig. 3. (a) UV–vis diffuse reflectance spectra of BiOI TF (the inset image is plots of $(ahv)^{1/2}$ versus energy (hv)); (b) I–V curves of BiOI TF electrode (the inset image is the I–V curves of TiO_2 TF electrode).

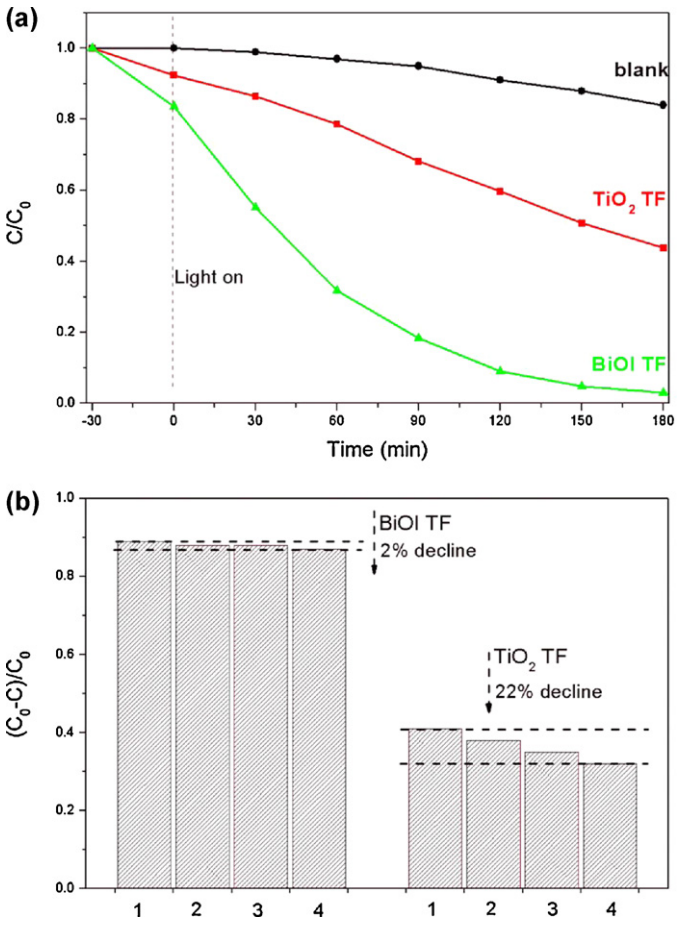

Fig. 4. (a) Photocatalytic activity of BiOI TF and TiO_2 TF for RhB photocatalytic degradation under Xenon lamp irradiation; and (b) cycle runs in the photocatalytic degradation of RhB for 2 h under Xenon lamp irradiation.

evaluated by the performance parameters of short circuit photocurrent densities (J_{sc}), open circuit potentials (V_{oc}) and fill factors (FF). The J_{sc} (1.52 mA cm^{-2}) and η (0.134%) of BiOI TF electrode were more than seventy and thirty times of that of reported result (J_{sc} = 0.02 mA cm^{-2} and η = 0.004%).[28,29] The good photoelectrochemical performance may be come from two factors: the self-induced internal electric fields of BiOI and CVT process, which result in high separation efficiency of photogenerated charges. On the base of above DRS and photoelectrochemical results, BiOI should be a potential sunlight photocatalyst material for solar application.

3.2. Photocatalytic activity and durability

The photocatalytic activity of the BiOI TF was measured on the photocatalytic degradation of RhB (Fig. 4a). As a comparison, direct photolysis of RhB was also performed using bare FTO substrate. It was observed the direct photolysis of RhB was 10% at 180 min. Although the as-synthesized BiOI TF had a thickness (690 nm, Fig. 2b) much thinner than that of the TiO_2 TF (thickness is 8 μm, Fig. S5), BiOI TF displayed higher photocatalytic activity than TiO_2 TF. And it demonstrated about 2 times higher photoactivity, in comparison to TiO_2 TF. The degradation ratio was 90% for BiOI TF at 120 min, while degradation ratio of 38% was obtained by TiO_2 TF. Total organic carbon (TOC) degradation was also used to prove the CO_2 production of RhB degradation (Fig. S6). The TOC removal rate of the solution reached 52.6% within 120 min BiOI TF, indicating that the as-prepared BiOI TF showed high photocatalytic efficiency in mineralizing organic pollutants than TiO_2 TF (29.4%). This high photocatalytic activity is in agreement with the above good photoelectrochemical performance. In photocatalysis systems, the pH value is one of the factors influencing the rate of degradation. For, BiOI TF, it is clearly observed that with the decreasing of pH, the photocatalytic rate is also increased (Fig. S7). It is because that the H^+ can promote the hydroxyl radical (•OH, an important reactive oxygen species for dyes degradation) production via a two-electron oxidation pathway[30] and this result is in agreement with previous reports about BiOCl and $BiVO_4$.[31,32]

On the other hand, durability is an important factor for photocatalyst in practical applications. Photocatalysis would not be employed if its photocatalytic activity could not possess a long lifetime.[20] In the durability experiments, BiOI TF and TiO_2 TF were further examined for another three cycles. The results showed that BiOI TF showed high applied value in photocatalysis for the durability (Fig. 4c) with only 2% decline of photocatalytic activity after 4 times cycle. However, the photocatalytic activity of TiO_2 TF decrease 22% after 4 times cycle. The higher photocatalytic durability might benefit from the stronger junction between the BiOI TF and the FTO substrate by CVT immobilization. However, the adherence between the TiO_2 TF and the FTO substrate was relatively weak. Therefore, BiOI TF showed better durability than TiO_2 TF for photocatalytic performance in RhB degradation.

3.3. Photocatalytic selectivity

By analyzing the UV–vis absorption spectra during the photocatalytic degradation of RhB with BiOI TF, we found that the

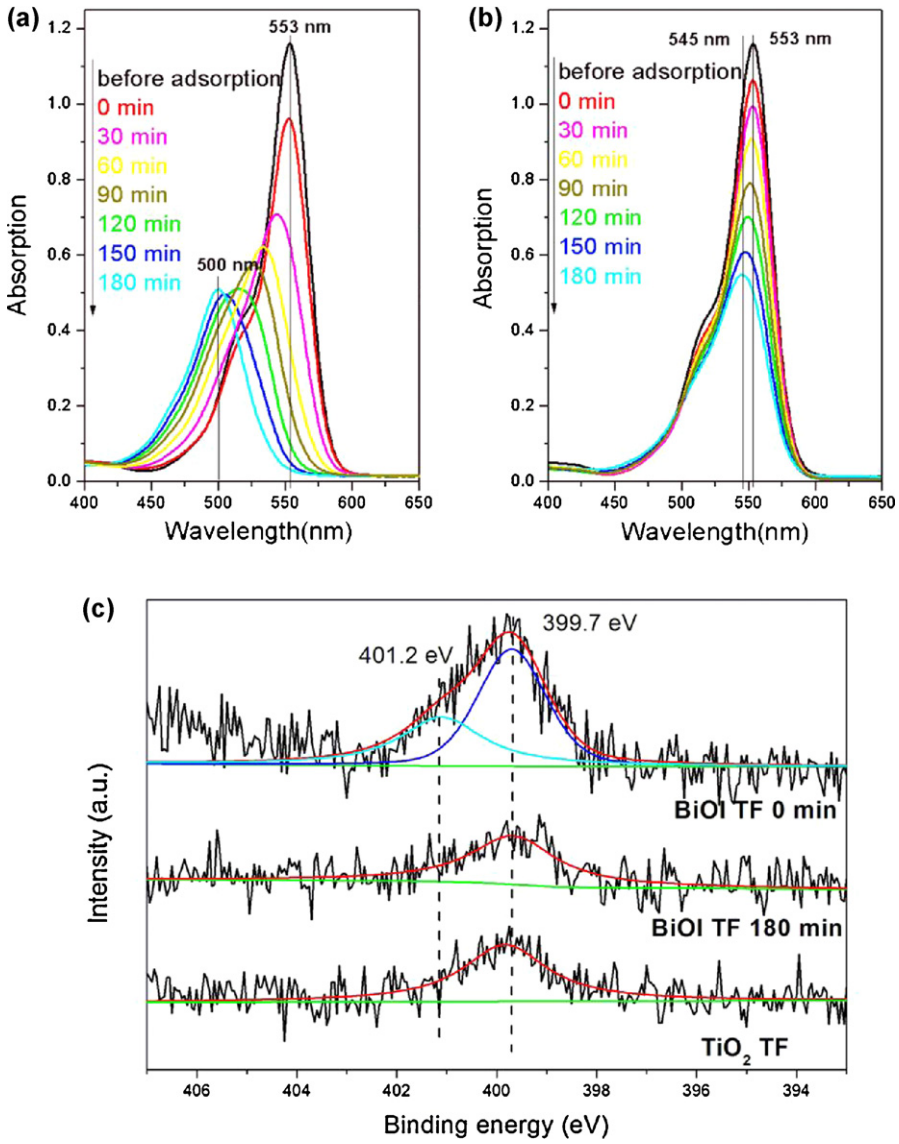

Fig. 5. Temporal UV–vis absorption spectra during the photocatalytic degradation of RhB with BiOI TF (a) and TiO_2 TF (b) under Xenon lamp irradiation; (c) N 1s XPS spectra of RhB adsorbed on BiOI (before and after Xenon lamp irradiation) and RhB adsorbed on TiO_2.

noticeable difference in the spectral changes between the TiO_2 TF and BiOI TF systems. The extents of the blue shift in the characteristic absorption peak of RhB. In the case of TiO_2 TF, blue shift of the characteristic absorption peak was little (from 554 to 545 nm, Fig. 5b). By contrast, the characteristic absorption peak of RhB exhibited a marked blue shift (from 554 to 500 nm, Fig. 5a) in the BiOI TF system. This difference implies that the prevailing PCD path of the RhB is N-de-ethylation. It was well recorded that the RhB photodegradation occurred via two competitive processes: N-de-ethylation and the destruction of the conjugated structure. The N 1s XPS spectrums of RhB which adsorbed on TiO_2 and BiOI are shown in Fig. 5c. The XPS peak of N 1s in pure solid RhB dye is located at 399.3 eV.[33] The N 1s peak of RhB adsorbed on TiO_2 has 0.3 eV shift to a higher binding energy (399.7 eV). Once RhB is adsorbed on the surface of BiOI, a new peak appears at 401.1 eV, and the shift is about 1.4 eV relative to RhB on pure TiO_2 and 1.8 eV relative to pure RhB respectively. The shift results from the interaction between the {0 0 1} facets of BiOI and the N+ group of RhB. So, the {0 0 1} facets of BiOI are negative which is in agreement with the surface atoms structure: 100% terminal oxygen atoms. Therefore, it can be concluded that BiOI displays sorption selectivity for azo dyes, and result in high photocatalytic selectivity. On the other hand, it can be seen that the new peak at 401.1 eV disappeared after 180 min irradiation. It proved the existence of N-de-ethylation process for RhB adsorbed on the surface of BiOI.

The photocatalytic selectivity of the BiOI TF and TiO_2 TF was investigated by photocatalytic degradation of a mixed MB (cationic dye with N+ and S+ group) and MO (anionic dye with O— group) aqueous solution (Fig. 6 and Fig. S8). For TiO_2 TF, the degradation rate of MB is close to that of MO. And the selective photocatalytic ability R ($R = k_{MB}/k_{MO}$) is 1.1. In contrast, the degradation rates of MB are much faster than those of MO for BiOI TF, confirming a preferential degradation of MB. And the selective photocatalytic ability R is 6.9 which are 6 times higher than TiO_2 TF. This result indicates that BiOI TF with {0 0 1} facets exposing is a high selective photocatalysis.

3.4. Photocatalytic mechanism

Fig. 7a shows the trapping experiment of active species during the photocatalytic reaction under Xenon lamp irradiation. It can be seen that the photocatalytic degradation of RhB was not affected

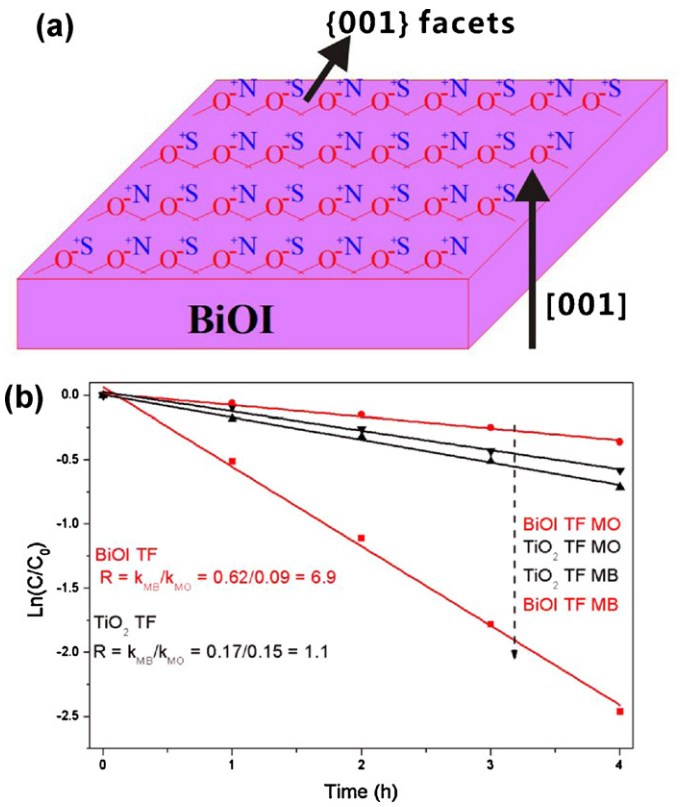

Fig. 6. (a) Modle of selective adsorption of BiOI; (b) a comparison of photocatalytic selectivity of BiOI TF and TiO_2 TF under Xenon lamp irradiation.

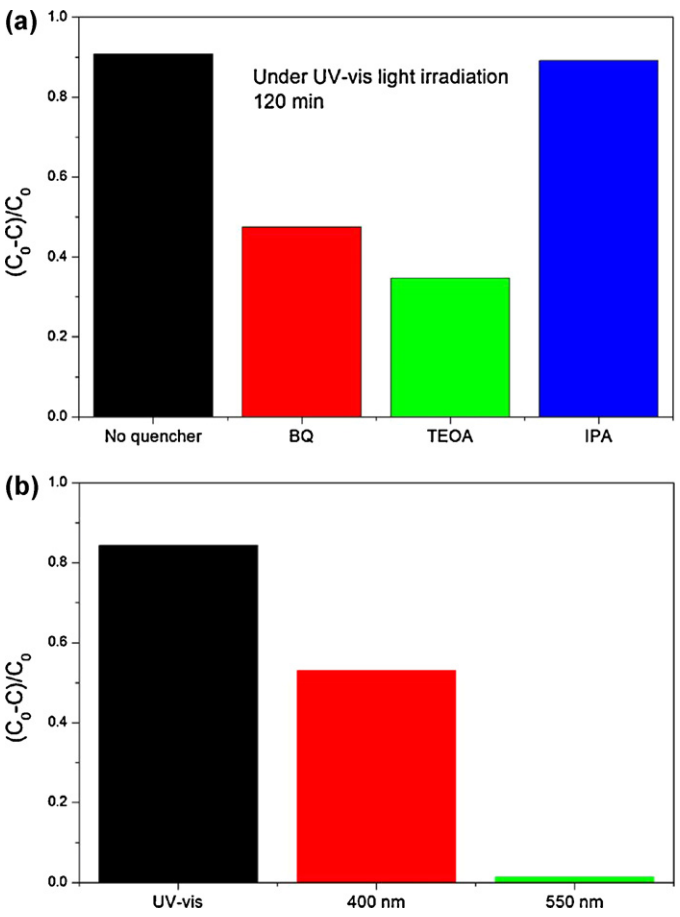

Fig. 7. Photocatalytic mechanism for BiOI TF: (a) trapping experiment of active species during the photocatalytic reaction with 120 min Xenon lamp irradiation; and (b) transformation percentage of NBT concentration under Xenon lamp, 400 nm and 550 nm monochromatic light irradiation.

by the addition of 1 mM IPA (a quencher of •OH). On the contrary, the photocatalytic degradation of RhB decreased obviously with the addition BQ (a quencher of $O_2^{\bullet-}$) and TEOA (a quencher of h+). Therefore, it can be concluded that $O_2^{\bullet-}$ and h^+ are the main active species rather than •OH under Xenon lamp irradiation. In addition, a colorless molecular probe, nitroblue tetrazolium (NBT) was chosen to quantify the $O_2^{\bullet-}$ concentration (NBT transformation percentage, Fig. 7b). It also proved the generation of $O_2^{\bullet-}$ under Xenon lamp irradiation. It is in agreement with the results of trapping experiments.

The valence band maximum (VBM) of BiOI had been calculated according to an empirical equation: $E_{CBM} = \chi - E_e - 0.5E_g$, where E_{CBM} is the CBM edge potential; χ is the electronegativity of the semiconductor, which is the geometric mean of the electronegativity of the constituent atoms; E_e is the energy of free electrons on the hydrogen scale (about 4.5 eV); E_g is the band gap energy of the semiconductor; and EVBM can be determined by $E_{VBM} = E_{CBM} + E_g$.[12,26,34] As shown in Scheme 2, the CBM and VBM potentials are 0.6 eV and 2.39 eV, respectively. Because the standard redox potential of BiV/BiIII (+1.59 V) is more negative than that of •OH/OH− (+1.99 V).[22] So, there are no •OH production and photogenerated holes directly photocatalytic oxidize RhB as shown in Fig. 7a and b.

However, it is very surprised that $O_2^{\bullet-}$ was generated when the CBM potential of BiOI is more positive than $E_0(O_2/O_2^{\bullet-})$ (−0.046 eV vs NHE). The possible reason was shown in Scheme 2. When Xenon lamp irradiation, the high-energy part (irradiation energy is higher than 2.44 eV (508 nm)) can result in the photogenerated electrons exciting up to a reformed higher CBM potential than $E_0(O_2/O_2^{\bullet-})$ (−0.046 eV). Therefore, the electrons on the CBM of BiOI can react with O_2 to produce $O_2^{\bullet-}$. And the low-energy part (irradiation energy is lower than 2.44 eV) cannot induce the $O_2^{\bullet-}$ generation because the reformed CBM potential is lower than the CBM potential than $E_0(O_2/O_2^{\bullet-})$ (−0.046 eV). For proving the suggested reformed CBM photocatalytic mechanism of BiOI, monochromatic light wavelength of 400 and 550 nm were used to detect $O_2^{\bullet-}$ (Fig. 7b). It can bee found that there are $O_2^{\bullet-}$ production under 400 nm light irradiation and no $O_2^{\bullet-}$ under 550 nm light irradiation. These results indicate that the CBM potential BiOI is not the necessary condition for $O_2^{\bullet-}$ production. The similar reformed CBM photocatalytic mechanism also was happened on BiOCl and

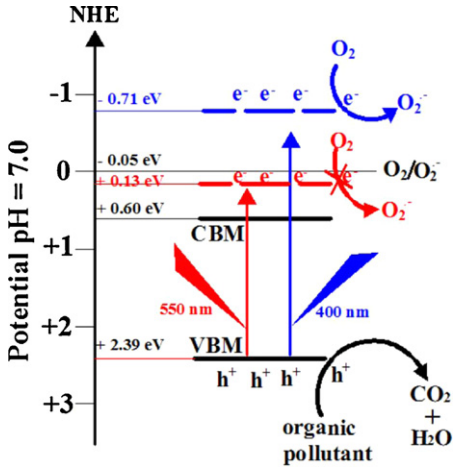

Scheme 2. Photocatalytic mechanism scheme of BiOI under Xenon lamp irradiation.

BiOBr.[27,35,36] It may be due to their same layered structure, and more studies also are need.

4. Conclusion

In conclusion, BiOI TF was prepared by a low temperature CVT route. As-synthesized BiOI nanosheets showed high symmety and the dominant exposed {0 0 1} facets and BiOI TF showed higher photocatalytic activity, durability and selectivity than P25 TiO_2 thin film. The layered structure and good photoelectrochemical performance, CVT immobilization, the 100% terminal oxygen atoms of {0 0 1} facets of BiOI are the origins for higher photocatalytic activity, durability and selectivity, respectively. A simple BiOI TF photocatalyst enhances three important factors of photocatalytic reaction. It provides a new opportunity to develop high photocatalytic activity, durability and selectivity sunlight photocatalyst in practical applications as an environmental friendly method. And photocatalytic mechanism results indicated that $O_2^{\bullet -}$ and h^+ are the main active species under high-pressure Xenon lamp irradiation. And corresponding reformed CBM photocatalytic mechanism was suggested.

Acknowledgements

This work was supported by National Natural Science Foundation of China (Nos: 21273164, 21271146 and 20973128) and Open Foundation of Key Laboratory of Catalysis and Materials Science of the State Ethnic Affairs Commission and ministry of education, south-central university for nationalities. The authors acknowledge the assistance from Center for Electron Microscopy, Wuhan University.

Appendix A. Supplementary data

Supplementary data associated with this article can be found, in the online version, at http://dx.doi.org/10.1016/j.apcatb.2012.10.011.

References

[1] A. Kubacka, M. Fernández-García, G. Colón, Chemical Reviews 112 (2012) 1555–1614.
[2] X. Chen, S.L. Shen, L. Guo, S.S. Mao, Chemical Reviews 110 (2010) 6503–6570.
[3] K.L. Zhang, C.M. Liu, F.Q. Huang, C. Zheng, W.D. Wang, Applied Catalysis B: Environmental 68 (2006) 125–129.
[4] L. Ye, L. Tian, T. Peng, L. Zan, Journal of Materials Chemistry 21 (2011) 12419–12484.
[5] X. Xiao, W.D. Zhang, Journal of Materials Chemistry 20 (2010) 5866–5870.
[6] Y. Li, J. Wang, H. Yao, L. Dang, Z. Li, Catalysis Communications 12 (2011) 660–664.
[7] Y. Li, J. Wang, H. Yao, L. Dang, Z. Li, Journal of Molecular Catalysis A: Chemical 334 (2011) 116–122.
[8] W.L. Huang, Q. Zhu, Journal of Computational Chemistry 30 (2009) 183–190.
[9] X. Zhang, L. Zhang, Journal of Physical Chemistry C 114 (2010) 18198–18206.
[10] L. Ye, L. Zan, L. Tian, T. Peng, J. Zhang, Chemical Communications 47 (2011) 6951–6953.
[11] J. Jiang, K. Zhao, X. Xiao, L. Zhang, Journal of the American Chemical Society 134 (2012) 4473–4476.
[12] X. Zhang, Z. Ai, F. Jia, L. Zhang, Journal of Physical Chemistry C 112 (2008) 747–753.
[13] X. Chang, J. Huang, C. Cheng, Q. Sui, W. Sha, G. Ji, S. Deng, G. Yu, Catalysis Communications 11 (2010) 460–464.
[14] Y. Lei, G. Wang, S. Song, W. Fan, M. Pang, J. Tang, H. Zhang, Dalton Transactions 39 (2010) 3273–3278.
[15] J. Henle, P. Simon, A. Frenzel, S. Scholz, S. Kaskel, Chemistry of Materials 19 (2007) 366–373.
[16] H. Peng, C.K. Chan, S. Meister, X.F. Zhang, Y. Cui, Chemistry of Materials 21 (2009) 247–252.
[17] P. Dai, X. Shen, Z. Lin, Z. Feng, H. Xua, J. Zhan, Chemical Communications 46 (2010) 5749–5751.
[18] K. Ramasamy, M.A. Malik, P. O'Brien, Chemical Science 2 (2011) 1170–1172.
[19] C.S. Mcnally, D.P. Turner, A.N. Kulak, F.C. Meldrum, G. Hyett, Chemical Communications 48 (2012) 1490–1492.
[20] Q. Mu, Q. Zhang, H. Wang, Y. Li, J. Mater. Chem. doi:10.1039/C2JM32781C.
[21] M. Zhang, C. Chen, W. Ma, J. Zhao, Angewandte Chemie International Edition 47 (2008) 9730–9733.
[22] M. Zhang, Q. Wang, C. Chen, L. Zang, W. Ma, J. Zhao, Angewandte Chemie 121 (2009) 6197–6200.
[23] S. Liu, J. Yu, M. Jaroniec, Journal of the American Chemical Society 132 (2010) 11914–11916.
[24] Q. Xiang, J. Yu, M. Jaroniec, Chemical Communications 47 (2011) 4532–4534.
[25] J. Zhang, W. Chen, J. Xi, Z. Ji, Materials Letters 79 (2012) 259–262.
[26] L. Ye, J. Liu, C. Gong, L. Tian, T. Peng, L. Zan, ACS Catalysis 2 (2012) 1677–1683.
[27] L. Ye, K. Deng, F. Xu, L. Tian, T. Peng, L. Zan, Physical Chemistry Chemical Physics 14 (2012) 82–85.
[28] K. Wang, F. Jia, Z. Zheng, L. Zhang, Electrochemistry Communications 12 (2010) 1764–1767.
[29] K. Zhao, X. Zhang, L. Zhang, Electrochemistry Communications 11 (2009) 612–615.
[30] Y. Cui, J. Huang, X. Fu, X. Wang, Catalysis Science and Technology 2 (2012) 1396–1402.
[31] B. Pare, B. Sarwan, S.B. Jonnalagadda, Journal of Molecular Structure 1007 (2012) 196–202.
[32] A. Martıĭnez-de la Cruz, U.M. Garcı'a Peĭrez, Materials Research Bulletin 45 (2010) 135–141.
[33] Q. Wang, C. Chen, D. Zhao, W. Ma, J. Zhao, Langmuir 24 (2008) 7338–7345.
[34] X. Zhang, L. Zhang, T. Xie, D. Wang, Journal of Physical Chemistry C 113 (2009) 7371–7378.
[35] M.A. Gondal, X. Chang, M.A. Ali, Z.H. Yamani, Q. Zhou, G. Ji, Applied Catalysis A: General 397 (2011) 192–200.
[36] Z. Jiang, F. Yang, G. Yang, L. Kong, M.O. Jones, T. Xiao, P.P. Edwards, Journal of Photochemistry and Photobiology A: Chemistry 212 (2010) 8–13.